

---

# Interpreting and Improving Diffusion Models Using the Euclidean Distance Function

---

**Frank Permenter**

Toyota Research Institute  
Cambridge, MA 02139  
frank.permenter@tri.global

**Chenyang Yuan**

Toyota Research Institute  
Cambridge, MA 02139  
chenyang.yuan@tri.global

## Abstract

Denoising is intuitively related to projection. Indeed, under the manifold hypothesis, adding random noise is approximately equivalent to orthogonal perturbation. Hence, learning to denoise is approximately learning to project. In this paper, we use this observation to reinterpret denoising diffusion models as approximate gradient descent applied to the Euclidean distance function. We then provide straight-forward convergence analysis of the DDIM sampler under simple assumptions on the projection-error of the denoiser. Finally, we propose a new sampler based on two simple modifications to DDIM using insights from our theoretical results. In as few as 5-10 function evaluations, our sampler achieves state-of-the-art FID scores on pretrained CIFAR-10 and CelebA models and can generate high quality samples on latent diffusion models.

## Introduction

Diffusion models achieve state-of-the-art quality on many image generation tasks [35, 37, 38]. They are also successful in text-to-3D generation [32, 16] and novel view synthesis [25]. Outside the image domain, they have been used for robot path-planning [15, 2], prompt-guided human animation [47], and text-to-audio generation [20, 34].

Diffusion models are presented as the reversal of a stochastic process that corrupts clean data with increasing levels of random noise [42, 14]. This reverse process can also be interpreted as likelihood maximization of a noise-perturbed data-distribution using learned gradients (called *score functions*) [45, 46]. While these interpretations are inherently probabilistic, the samplers widely used in practice are often deterministic [43, 28, 24, 52]. In this paper, we tackle this divide and provide a deterministic framework for reasoning about, improving and potentially discovering new applications of diffusion models.

For our first contribution, we reinterpret diffusion models as *projection* onto the *support* of the training-set distribution, discarding the underlying measure. This deterministic interpretation is based on an approximate correspondence between denoising and projection (noted in [7, 36]) that we make rigorous in Section 2, assuming the manifold hypothesis. We then reinterpret sampling as approximate gradient descent on the Euclidean distance-function and perform convergence analysis under a simple error model relating denoising and projection (Section 3). This analysis also provides rigorous justification for log-linear noise schedules. Finally, we leverage properties of the distance function to design a high-order sampler that aggregates previous denoiser outputs to reduce error (Section 4).

We conclude with computational evaluation of our sampler (Section 5) that demonstrates state-of-the-art FID scores on pretrained CIFAR-10 and CelebA datasets and comparable results to the best samplers for high-resolution latent models such as Stable Diffusion (Figure 1). Section 6 provides

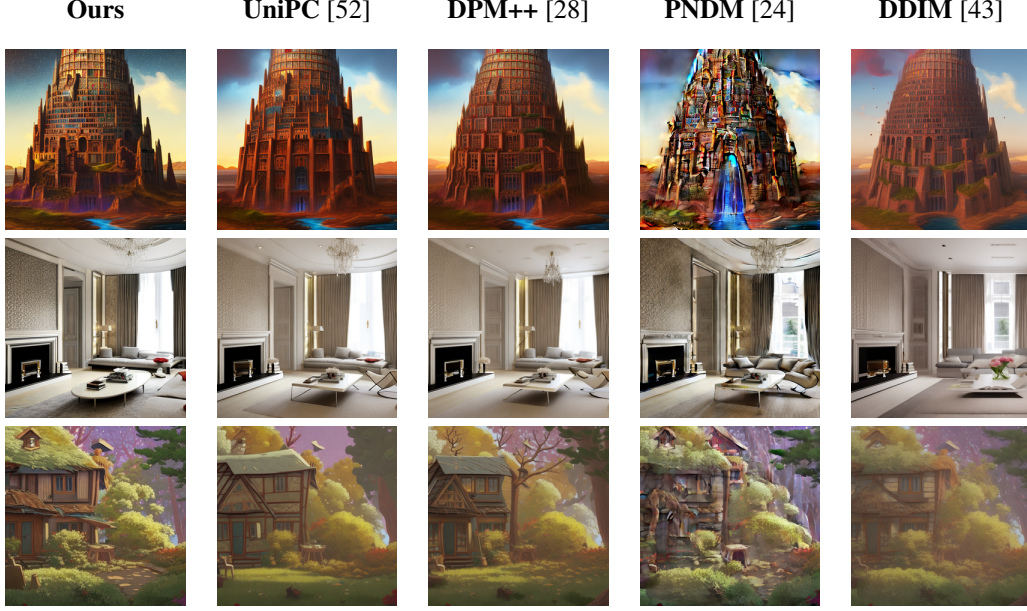


Figure 1: Example outputs of our sampler on text-to-image Stable Diffusion compared to other commonly used samplers, when limited to  $N = 10$  function evaluations.

novel interpretations of existing techniques under the framework of distance functions and outlines directions for future research.

## 1 Background

Denoising diffusion models (along with all other generative models) treat datasets as samples from a probability distribution supported on a subset  $\mathcal{K}$  of  $\mathbb{R}^n$ . They are used to *generate* new points in  $\mathcal{K}$  outside the training set. We overview their basic features. We then state properties of the Euclidean distance function  $\text{dist}_{\mathcal{K}}(x)$  that are key to our contributions.

### 1.1 Denoising Diffusion Models

**Denoisers** Denoising diffusion models are trained to estimate a *noise vector*  $\epsilon \in \mathbb{R}^n$  from a given  $y \in \mathbb{R}^n$  and  $\sigma > 0$  such that  $y = x + \sigma\epsilon$  approximately holds for some  $x$  in the training-set. The learned function, denoted  $\epsilon_{\theta} : \mathbb{R}^n \times \mathbb{R}_{+} \rightarrow \mathbb{R}^n$ , is called a *denoiser*. The trainable parameters, denoted jointly by  $\theta \in \mathbb{R}^m$ , are found by (approximately) minimizing

$$L(\theta) := \mathbf{E}_{x, \sigma, \epsilon} \|\epsilon_{\theta}(x + \sigma\epsilon, \sigma) - \epsilon\|^2 \quad (1)$$

when  $x$  is drawn from the training-set distribution,  $\sigma$  is drawn uniformly from a finite set of positive numbers, and  $\epsilon$  is drawn from a Gaussian distribution  $\mathcal{N}(0, I)$ . In practice, training is done by applying gradient descent to  $\|\epsilon_{\theta}(x + \sigma\epsilon, \sigma) - \epsilon\|^2$  using randomly sampled  $(x, \epsilon, \sigma)$ .

Throughout, we let  $\{\sigma_t\}_{t=0}^N$  denote the set of  $\sigma$  and assume that  $\sigma_t > \sigma_{t-1}$ . For simplicity of notation we use  $\epsilon_{\theta}(y, \sigma_t)$  and  $\epsilon_{\theta}(y, t)$  interchangeably based on context. The sequence of  $\sigma_t$  is the basis of *sampling algorithms* we overview next.

**Sampling** Given  $y$ , the estimated noise  $\epsilon_{\theta}(y, \sigma)$  induces an estimate of  $\hat{x}_0 \in \mathcal{K}$  via

$$\hat{x}_0(y, \sigma) := y - \sigma\epsilon_{\theta}(y, \sigma). \quad (2)$$

Aiming to improve accuracy, sampling algorithms construct a sequence  $\hat{x}_0^t := \hat{x}_0(x_t, \sigma_t)$  of estimates that in turn arises from a sequence of points  $x_t$  initialized at a given  $x_N$ . The most basic samplers recursively construct  $x_{t-1}$  from  $x_t$  and  $\epsilon_{\theta}(x_t, \sigma_t)$ . For instance, the DDPM [14] sampler uses the

recursion

$$x_{t-1} = x_t + (\sigma_{t'} - \sigma_t)\epsilon_\theta(x_t, \sigma_t) + \eta w_t, \quad (3)$$

where  $w_t \sim \mathcal{N}(0, I)$ ,  $\sigma_{t'} = \sigma_{t-1}^2/\sigma_t$  and  $\eta = \sqrt{\sigma_{t-1}^2 - \sigma_{t'}^2}$ . (Note that by definition  $\sigma_{t'} < \sigma_{t-1} < \sigma_t$ , as  $\sigma_{t-1}$  is the geometric mean of  $\sigma_{t'}$  and  $\sigma_t$ .) The DDIM [43] sampler, on the other hand, uses the recursion

$$x_{t-1} = x_t + (\sigma_{t-1} - \sigma_t)\epsilon_\theta(x_t, \sigma_t). \quad (4)$$

Note that DDPM is randomized given the samples  $w_t$  whereas DDIM is deterministic. Note also these samplers were originally presented in variables  $z_t$  satisfying  $z_t = \sqrt{\alpha_t}x_t$ , where  $\alpha_t$  satisfies  $\sigma_t^2 = \frac{1-\alpha_t}{\alpha_t}$ . We prove equivalence of the original definitions to (3) and (4) in Appendix A and note that the change-of-variables from  $z_t$  to  $x_t$  previously appears in [46, 18, 43].

## 1.2 Distance, Projection, and Reach

The *distance function* of a set  $\mathcal{K} \subseteq \mathbb{R}^n$ , denoted  $\text{dist}_{\mathcal{K}} : \mathbb{R}^n \rightarrow \mathbb{R}$ , is defined via

$$\text{dist}_{\mathcal{K}}(x) := \inf\{\|x - y\| : y \in \mathcal{K}\}. \quad (5)$$

The *projection* of  $x \in \mathbb{R}^n$ , denoted  $\text{proj}_{\mathcal{K}}(x)$ , is the set of points that attain this distance, i.e.,

$$\text{proj}_{\mathcal{K}}(x) := \{y \in \mathcal{K} : \text{dist}_{\mathcal{K}}(x) = \|x - y\|\}. \quad (6)$$

When  $\text{proj}_{\mathcal{K}}(x)$  is a singleton, i.e., when  $\text{proj}_{\mathcal{K}}(x) = \{y\}$ , we abuse notation and let  $\text{proj}_{\mathcal{K}}(x)$  denote  $y$ . We collect useful facts below.

**Proposition 1.1** (page 283, Theorem 3.3 of [9]). *Suppose  $\mathcal{K} \subseteq \mathbb{R}^n$  is closed and  $x \notin \mathcal{K}$ . If  $\text{proj}_{\mathcal{K}}(x)$  is a singleton, then the following statements hold:*

- *The gradient  $\nabla \text{dist}_{\mathcal{K}}(x)$  exists and satisfies  $\nabla \text{dist}_{\mathcal{K}}(x) = \text{dist}_{\mathcal{K}}(x)^{-1}(x - \text{proj}_{\mathcal{K}}(x))$ . Further,  $\|\nabla \text{dist}_{\mathcal{K}}(x)\| = 1$ .*
- *The gradient of  $f(x) := \frac{1}{2}\text{dist}_{\mathcal{K}}(x)^2$  satisfies  $\nabla f(x) = \text{dist}_{\mathcal{K}}(x)\nabla \text{dist}_{\mathcal{K}}(x)$ . Equivalently,  $\nabla f(x) = x - \text{proj}_{\mathcal{K}}(x)$ .*

Further,  $\text{proj}_{\mathcal{K}}(x)$  is a singleton for almost all  $x \in \mathbb{R}^n$ .

Suppose that  $y = x + \sigma\epsilon$  for  $\epsilon \sim \mathcal{N}(0, I)$ . The unit vector  $\nabla \text{dist}_{\mathcal{K}}(y)$  is intuitively related to  $\epsilon$  whereas  $\text{dist}_{\mathcal{K}}(y)$  is intuitively related to  $\sigma$ . The next section establishes conditions when these quantities are approximately equal up-to scaling by  $\sqrt{n}$ . We'll state results using the *reach* of  $\mathcal{K}$ , defined as the largest  $\tau > 0$  such that  $\text{proj}_{\mathcal{K}}(x)$  is unique when  $\text{dist}_{\mathcal{K}}(x) < \tau$ . Local Lipschitz continuity of  $\text{proj}_{\mathcal{K}}(x)$  can also be established using  $\text{reach}(\mathcal{K})$ ; see Appendix B.

## 2 Manifold Hypothesis and Equivalence Between Denoising and Projection

The *manifold hypothesis* [4, 12, 33] asserts that “real-world” datasets are (approximately) contained in low-dimensional manifolds of  $\mathbb{R}^n$ . We next show that denoising is approximately equivalent to projection under a version of this hypothesis. Specifically, we suppose that  $\mathcal{K}$  is a manifold of dimension  $d$  with  $d \ll n$ . We then show that the denoiser  $\epsilon_\theta$  approximates  $\text{proj}_{\mathcal{K}}(y)$  with error that decreases with  $d$ . We leverage the following result, stated in terms of the normal space  $N_{\mathcal{K}}(x) \subseteq \mathbb{R}^n$ , a subspace of dimension  $n - d$ .

**Lemma 2.1** (Theorem 4.8(12) [11]). *If  $\|w\| < \text{reach}(\mathcal{K})$  and  $w \in N_{\mathcal{K}}(x)$ , then  $\text{proj}_{\mathcal{K}}(x + w) = x$ .*

Decomposing  $w$  using  $N_{\mathcal{K}}(x) \oplus (N_{\mathcal{K}}(x))^\perp$  and combining Lemma 2.1 with Gaussian concentration inequalities [48, Chapter 3] provides a *backward error* bound on the approximation  $\text{proj}_{\mathcal{K}}(x + w) \approx x$ . Invoking Lipschitz continuity of  $\text{proj}_{\mathcal{K}}(x + w)$  when  $\text{dist}_{\mathcal{K}}(x + w) < \text{reach}(\mathcal{K})$  provides a *forward error* bound. We state these bounds informally here, deferring precise statements and proofs to Appendix B.

**Theorem 2.1** (Denoising vs Projection (informal)). *Fix  $\sigma > 0$  and suppose that  $\text{reach}(\mathcal{K}) \gtrsim \sigma\sqrt{n}$ . Given  $x \in \mathcal{K}$  and  $\epsilon \sim \mathcal{N}(0, I)$ , let  $y = x + \sigma\epsilon$ . With high probability, we have:*

- (Backward error)  $x = \text{proj}_{\mathcal{K}}(y + \delta)$  for  $\delta \in \mathbb{R}^n$  satisfying  $\|\delta\| \leq \sigma\sqrt{d}$ .
- (Forward error)  $\|\text{proj}_{\mathcal{K}}(y) - x\| \lesssim \sigma\sqrt{d}$ .

The second statement illustrates that perfect denoising of  $y = x + \sigma\epsilon$  approximates  $\text{proj}_{\mathcal{K}}(y)$ . From Proposition 1.1, it is therefore natural to bound the approximation error of  $\epsilon_{\theta}(y, t) \approx \sqrt{n}\nabla \text{dist}_{\mathcal{K}}(y)$  and  $\sqrt{n}\sigma_t \approx \text{dist}_{\mathcal{K}}(y)$ , which together induces the approximation  $\text{proj}_{\mathcal{K}}(y) \approx y - \sigma_t\epsilon_{\theta}(y, t)$ . The next section incorporates precise versions of these approximations into sampling algorithms. We also note that prior analysis of diffusion under the manifold hypothesis includes [8].

### 3 Equivalence Between Sampling and Gradient Descent

Section 2 establishes that denoising approximates projection. We now study DDIM under two different approximation models. Letting  $f(x) := \frac{1}{2}\text{dist}_{\mathcal{K}}(x)^2$  and noting that  $\nabla f(x) = x - \text{proj}_{\mathcal{K}}(x)$  when  $\nabla f(x)$  exists, we state these models as the following assumptions.

**Assumption 1** (Exact projection). *If  $(x, t)$  satisfies  $\text{dist}_{\mathcal{K}}(x) = \sqrt{n}\sigma_t$  and  $\nabla f(x)$  exists, then  $\sigma_t\epsilon_{\theta}(x, \sigma_t) = \nabla f(x)$ .*

**Assumption 2** (Projection with relative error). *There exists  $\nu \geq 1$  and  $\eta \geq 0$  such that if  $\frac{1}{\nu}\text{dist}_{\mathcal{K}}(x) \leq \sqrt{n}\sigma_t \leq \nu\text{dist}_{\mathcal{K}}(x)$  and  $\nabla f(x)$  exists, then  $\|\sigma_t\epsilon_{\theta}(x, t) - \nabla f(x)\| \leq \eta\text{dist}_{\mathcal{K}}(x)$ .*

Assumption 1 assumes that denoising is precisely projection. Assumption 2 weakens exactness to a relative-error assumption on  $\nabla f(x)$  given that  $\|\nabla f(x)\| = \text{dist}_{\mathcal{K}}(x)$ . We first show that DDIM is precisely gradient descent with step-size determined by  $\sigma_t$  under Assumption 1. We then interpret DDIM as gradient descent with relative-error under Assumption 2 and provide simple convergence analysis. Proofs are postponed to Appendix C.

#### 3.1 Exact Projection and Gradient Descent

We use the following lemma for gradient descent applied to the squared-distance function  $f(x)$ .

**Lemma 3.1.** *Fix  $x \in \mathbb{R}^n$  and suppose that  $\nabla f(x)$  exists. For step-size  $0 < \beta \leq 1$  consider the gradient descent iteration applied to  $f(x)$ :*

$$x_+ := x - \beta\nabla f(x)$$

*Then,  $\text{dist}_{\mathcal{K}}(x_+) = (1 - \beta)\text{dist}_{\mathcal{K}}(x) < \text{dist}_{\mathcal{K}}(x)$ .*

We can now characterize DDIM as follows.

**Theorem 3.1.** *Let  $x_N, x_{N-1}, \dots, x_0$  denote a sequence (18) generated by DDIM and suppose that Assumption 1 holds. Further suppose that  $\text{dist}(x_N) = \sqrt{n}\sigma_N < \text{reach}(\mathcal{K})$ . Then the following statements hold:*

- *The gradient of  $f(x) := \frac{1}{2}\text{dist}_{\mathcal{K}}(x)^2$  exists for all  $x_t$ . Further,  $x_t$  equals the sequence generated by gradient descent with step-size  $\beta_t := (1 - \sigma_{t-1}/\sigma_t)$ , i.e.,*

$$x_{t-1} = x_t - \beta_t\nabla f(x_t)$$

- *$\text{dist}_{\mathcal{K}}(x_t) = \sqrt{n}\sigma_t$  for all  $t$ .*

We remark that  $\text{dist}(x_N) < \text{reach}(\mathcal{K})$  is assumed only to guarantee existence of  $\nabla f(x_t)$  for each  $t$ . If relaxed, this theorem still holds generically.

#### 3.2 Approximate Projection and Gradient Descent with Error

Our relative-error model (Assumption 2) supposes that  $\frac{1}{\nu}\text{dist}_{\mathcal{K}}(x) \leq \sqrt{n}\sigma_t \leq \nu\text{dist}_{\mathcal{K}}(x)$ . To ensure this condition holds at each DDIM iteration, we need to lower and upper bound distance. For this, we use the following two lemmas.

**Lemma 3.2.** *The distance function  $\text{dist}_{\mathcal{K}} : \mathbb{R}^n \rightarrow \mathbb{R}$  for  $\mathcal{K} \subseteq \mathbb{R}^n$  satisfies*

$$\text{dist}_{\mathcal{K}}(u) - \|u - v\| \leq \text{dist}_{\mathcal{K}}(v) \leq \text{dist}_{\mathcal{K}}(u) + \|u - v\|$$

*for all  $u, v \in \mathbb{R}^n$ .*

**Lemma 3.3.** For  $\mathcal{K} \subseteq \mathbb{R}^n$ , let  $f(x) := \frac{1}{2} \text{dist}_{\mathcal{K}}(x)^2$ . The following statements hold.

- (a) If  $x_+ = x - \beta(\nabla f(x) + e)$  for  $e$  satisfying  $\|e\| \leq \eta \text{dist}_{\mathcal{K}}(x)$  and  $0 \leq \beta \leq 1$ , then  $(1 - \beta(\eta + 1)) \text{dist}_{\mathcal{K}}(x) \leq \text{dist}_{\mathcal{K}}(x_+) \leq (1 + \beta(\eta - 1)) \text{dist}_{\mathcal{K}}(x)$
- (b) If  $x_{t-1} = x_t - \beta_t(\nabla f(x_t) + e_t)$  for  $e_t$  satisfying  $\|e_t\| \leq \eta \text{dist}_{\mathcal{K}}(x_t)$  and  $0 \leq \beta_t \leq 1$ , then

$$\text{dist}_{\mathcal{K}}(x_N) \prod_{i=t}^N (1 - \beta_i(\eta + 1)) \leq \text{dist}_{\mathcal{K}}(x_{t-1}) \leq \text{dist}_{\mathcal{K}}(x_N) \prod_{i=t}^N (1 + \beta_i(\eta - 1))$$

From Lemma 3.3, the following condition ensures that  $\frac{1}{\nu} \text{dist}_{\mathcal{K}}(x) \leq \sqrt{n} \sigma_t \leq \nu \text{dist}_{\mathcal{K}}(x)$  holds at each DDIM iteration, leveraging the DDIM property that  $\sigma_{t-1} = (1 - \beta_t) \sigma_t$ .

**Definition 3.1.** We say that parameters  $\{\sigma_t\}_{t=0}^N$  are  $(\eta, \nu)$ -admissible if, for all  $t \in \{1, \dots, N\}$ ,

$$\frac{1}{\nu} \prod_{i=t}^N (1 + \beta_i(\eta - 1)) \leq \prod_{i=t}^N (1 - \beta_i) \leq \nu \prod_{i=t}^N (1 - \beta_i(\eta + 1)), \quad (7)$$

where  $\beta_t := 1 - \sigma_{t-1}/\sigma_t$ .

We now give error bounds for DDIM under the assumption that the noise levels  $\sigma_t$  are admissible. We then study admissible sequences for which  $\sigma_{t-1}/\sigma_t$  is constant, which in turn implies that the DDIM step-size  $\beta_t$  is fixed (Theorem 3.1).

### 3.2.1 Error Bounds

Our main result under the relative-error model follows.

**Theorem 3.2** (DDIM with relative error). *Let Assumption 2 hold and suppose  $\{\sigma_t\}_{t=0}^N$  is  $(\eta, \nu)$ -admissible for  $0 \leq \eta < 1$  and  $\nu \geq 1$ . Let  $x_t$  denote the sequence generated by DDIM and suppose that  $\text{dist}(x_N) = \sqrt{n} \sigma_N < \text{reach}(\mathcal{K})$ . The following statements hold.*

- The gradient of  $f(x) := \frac{1}{2} \text{dist}_{\mathcal{K}}(x)^2$  exists for all  $x_t$ . Further,  $x_t$  is generated by approximate gradient descent iterations of the form Lemma 3.3-(b) with  $\beta_t = 1 - \sigma_{t-1}/\sigma_t$
- $\frac{1}{\nu} \text{dist}_{\mathcal{K}}(x_t) \leq \sqrt{n} \sigma_t \leq \nu \text{dist}_{\mathcal{K}}(x_t)$  for all  $t$ .
- $\text{dist}_{\mathcal{K}}(x_N) \prod_{i=t}^N (1 - \beta_i(\eta + 1)) \leq \text{dist}_{\mathcal{K}}(x_{t-1}) \leq \text{dist}_{\mathcal{K}}(x_N) \prod_{i=t}^N (1 + \beta_i(\eta - 1))$  where  $\beta_t := 1 - \sigma_{t-1}/\sigma_t$ .

As with Theorem 3.1, the reach assumption  $\text{dist}(x_N) < \text{reach}(\mathcal{K})$  is made to guarantee that  $\nabla f(x_t)$  exists for all  $t$ . If relaxed, this theorem still holds generically.

### 3.2.2 Admissible Log-Linear Schedules for DDIM

We next characterize admissible  $\sigma_t$  of the form  $\sigma_{t-1} = (1 - \beta) \sigma_t$  where  $\beta$  denotes a constant step-size. This illustrates that admissible  $\sigma_t$ -sequences not only exist, they can also be explicitly constructed from  $(\eta, \nu)$ .

**Theorem 3.3.** Fix  $\beta \in \mathbb{R}$  satisfying  $0 \leq \beta < 1$  and suppose that  $\sigma_{t-1} = (1 - \beta) \sigma_t$ . Then  $\sigma_t$  is  $(\eta, \nu)$ -admissible if and only if  $\beta \leq \beta_{*,N}$  where  $\beta_{*,N} := \frac{c}{\eta + c}$  for  $c := 1 - \nu^{-1/N}$ .

Suppose we fix  $(\eta, \nu)$  and choose, for a given  $N$ , the step-size  $\beta_{*,N}$ . It is natural to ask how the error bounds of Theorem 3.2 change as  $N$  increases. The following establishes the limiting behavior of the final output  $(\sigma_0, x_0)$  of DDIM.

**Theorem 3.4.** Let  $x_N, \dots, x_1, x_0$  denote the sequence generated by DDIM with  $\sigma_t$  satisfying  $\sigma_{t-1} = (1 - \beta_{*,N}) \sigma_t$  for  $\nu \geq 1$  and  $\eta > 0$ . The following statements hold

- $\lim_{N \rightarrow \infty} \sigma_0/\sigma_N = \lim_{N \rightarrow \infty} (1 - \beta_{*,N})^N = (1/\nu)^{1/\eta}$ .
- $\lim_{N \rightarrow \infty} \text{dist}_{\mathcal{K}}(x_0)/\text{dist}_{\mathcal{K}}(x_N) \leq \lim_{N \rightarrow \infty} (1 + (\eta - 1)\beta_{*,N})^N = (1/\nu)^{\frac{1-\eta}{\eta}}$

This theorem illustrates that final error, while bounded, need not converge to zero under our error model. This motivates heuristically updating the step-size from  $\beta_{*,N}$  to a full step ( $\beta = 1$ ) during the final DDIM iteration. We adopt this approach in our experiments (Section 5).

---

**Algorithm 1** DDIM sampler [43]

---

**Require:**  $(\sigma_N, \dots, \sigma_0)$ ,  $x_N \sim \mathcal{N}(0, I)$ ,  $\epsilon_\theta$   
**Ensure:** Compute  $x_0$  with  $N$  evaluations of  $\epsilon_\theta$   
**for**  $t = N, \dots, 1$  **do**  
 $x_{t-1} \leftarrow x_t + (\sigma_{t-1} - \sigma_t)\epsilon_\theta(x_t, \sigma_t)$   
**return**  $x_0$

---



---

**Algorithm 2** Our second-order sampler

---

**Require:**  $(\sigma_N, \dots, \sigma_0)$ ,  $x_N \sim \mathcal{N}(0, I)$ ,  $\epsilon_\theta$   
**Ensure:** Compute  $x_0$  with  $N$  evaluations of  $\epsilon_\theta$   
 $x_{N-1} \leftarrow x_N + (\sigma_{N-1} - \sigma_N)\epsilon_\theta(x_N, \sigma_N)$   
**for**  $t = N - 1, \dots, 1$  **do**  
 $\bar{\epsilon}_t \leftarrow 2\epsilon_\theta(x_t, \sigma_t) - \epsilon_\theta(x_{t+1}, \sigma_{t+1})$   
 $x_{t-1} \leftarrow x_t + (\sigma_{t-1} - \sigma_t)\bar{\epsilon}_t$   
**return**  $x_0$

---

## 4 Improving Deterministic Sampling Algorithms via Gradient Estimation

### 4.1 Gradient Invariant of the Distance Function

The gradient  $\nabla \text{dist}_\mathcal{K}(x)$  does not change direction along line segments between a point  $x$  and its projection  $\text{proj}_\mathcal{K}(x)$ , i.e., letting  $\hat{x} = \text{proj}_\mathcal{K}(x)$ ,

$$\nabla \text{dist}_\mathcal{K}(\theta x + (1 - \theta)\hat{x}) = \nabla \text{dist}_\mathcal{K}(x) \quad \forall \theta \in (0, 1]. \quad (8)$$

Hence,  $\epsilon_\theta(x, \sigma)$  should be constant on this line-segment under our assumption that  $\epsilon_\theta(x, \sigma) \approx \sqrt{n} \nabla \text{dist}_\mathcal{K}(x)$  when  $\text{dist}_\mathcal{K}(x) \approx \sqrt{n}\sigma$ . Precisely, for  $x_1$  and  $x_2$  on this line-segment, we should have

$$\epsilon_\theta(x_1, \sigma_{t_1}) \approx \epsilon_\theta(x_2, \sigma_{t_2}) \quad (9)$$

if  $t_i$  satisfies  $\text{dist}_\mathcal{K}(x_i) \approx \sqrt{n}\sigma_{t_i}$ . This property suggests combining previous denoiser outputs  $\{\epsilon_\theta(x_i, \sigma_i)\}_{i=t+1}^N$  to estimate  $\epsilon_t = \sqrt{n} \nabla \text{dist}_\mathcal{K}(x_t)$ . We next propose a practical *second-order method*<sup>1</sup> for this estimation that combines the current denoiser output with the previous. Note that recently introduced *consistency models*[44] penalize violation of (9) during *training*. Interpreting denoiser output as  $\nabla \text{dist}_\mathcal{K}(x)$  and invoking (8) offers an alternative justification for these models.

### 4.2 A Second-Order Method via Gradient Estimation

Let  $e_t(\epsilon) = \epsilon - \epsilon_\theta(x_t, \sigma_t)$  be the error of  $\epsilon_\theta(x_t, \sigma_t)$  when predicting  $\epsilon$ . To estimate  $\epsilon$  from  $\epsilon_\theta(x_t, \sigma_t)$ , we minimize the norm of this error concatenated over two time-steps. Precisely, letting  $y_t(\epsilon) = (e_t(\epsilon), e_{t+1}(\epsilon))$ , we compute

$$\bar{\epsilon}_t := \arg \min_{\epsilon} \|y_t(\epsilon)\|_W^2, \quad (10)$$

where  $W$  is a specified positive-definite weighting matrix. To choose  $W$ , we make two assumptions on the denoising error: the coordinates  $e_t(\epsilon)_i$  and  $e_t(\epsilon)_j$  are uncorrelated for all  $i \neq j$ , and  $e_t(\epsilon)_i$  is only correlated with  $e_{t+1}(\epsilon)_i$  for all  $i$ . In other words, we consider  $W$  of the form

$$W = \begin{bmatrix} aI & bI \\ bI & cI \end{bmatrix} \quad (11)$$

and next show that this choice leads to a simple rule for selecting  $\bar{\epsilon}$ . From the optimality conditions of the quadratic optimization problem (10), we get that

$$\bar{\epsilon}_t = \frac{a+b}{a+c+2b}\epsilon_\theta(x_t, \sigma_t) + \frac{c+b}{a+c+2b}\epsilon_\theta(x_{t+1}, \sigma_{t+1}).$$

Setting  $\gamma = \frac{a+b}{a+c+2b}$ , we get the update rule

$$\bar{\epsilon}_t = \gamma \epsilon_\theta(x_t, \sigma_t) + (1 - \gamma) \epsilon_\theta(x_{t+1}, \sigma_{t+1}). \quad (12)$$

When  $b \geq 0$ , the minimizer  $\bar{\epsilon}_t$  is a simple convex combination of denoiser outputs. When  $b < 0$ , we can have  $\gamma < 0$  or  $\gamma > 1$ , i.e., the weights in (12) can be negative (but still sum to 1). Negativity of the weights can be interpreted as cancelling positively correlated error ( $b < 0$ ) in the denoiser outputs. Also note we can implicitly search over  $W$  by directly searching for  $\gamma$ .

## 5 Experiments

---

<sup>1</sup>This method is second-order in the sense that the update step uses previous values of  $\epsilon_\theta$ , and should not be confused with second-order derivatives.

We evaluate modifications of DDIM (Algorithm 1) that leverage insights from Section 4.2 and Section 3.2.2. Following Section 4.2 we modify DDIM to use a second-order update that corrects for error in the denoiser output (Algorithm 2). Specifically, we use the Equation (12) update with  $\gamma = 2$ , which is empirically tuned (see Appendix D). A comparison of this update with DDIM is visualized in Figure 2. Following Section 3.2.2, we select a noise schedule  $(\sigma_N, \dots, \sigma_0)$  that decreases at a log-linear (geometric) rate. The specific rate is determined by an initial and target noise level. Our  $\sigma_t$  schedule is illustrated in Figure 3, along with other commonly used schedules. We note that log-linear schedules have been previously proposed for SDE-samplers [46]; to our knowledge we are the first to propose and analyze their use for DDIM<sup>2</sup>

All the experiments were run on a single Nvidia RTX 4090 GPU.

### 5.1 Evaluation of Noise Schedule

In Figure 3 we plot our schedule (with our choices of  $\sigma_t$  detailed in Appendix E) with three other commonly used schedules on a log scale. The first is the evenly spaced subsampling of the training noise levels used by DDIM. The second “DDIM Offset” uses the same even spacing but starts at a smaller  $\sigma_N$ , the same as that in our schedule. This type of schedule is typically used for guided image generation such as SDEdit [29]. The third “EDM” is the schedule used in [18, Eq. 5], with  $\sigma_{\max} = 80, \sigma_{\min} = 0.002$  and  $\rho = 7$ .

We then test these schedules on the DDIM sampler Algorithm 1 by sampling images with  $N = 10$  steps from the CIFAR-10 and CelebA models. We see that in Table 1 that our schedule improves the FID of the DDIM sampler on both datasets even without the second-order updates. This is in part due to choosing a smaller  $\sigma_N$  so the small number of steps can be better spent on lower noise levels (the difference between “DDIM” and “DDIM Offset”), and also because our schedule decreases  $\sigma_t$  at a faster rate than DDIM (the difference between “DDIM Offset” and “Ours”).

### 5.2 Evaluation of Full Sampler

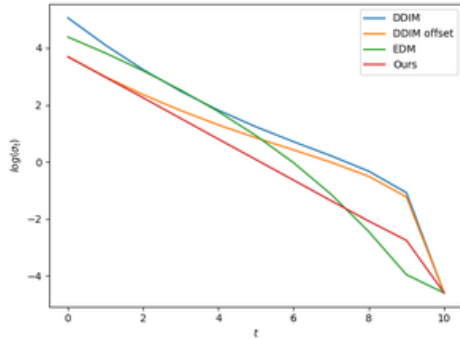


Figure 3: Plot of different choices of  $\log(\sigma_t)$  for  $N = 10$ .

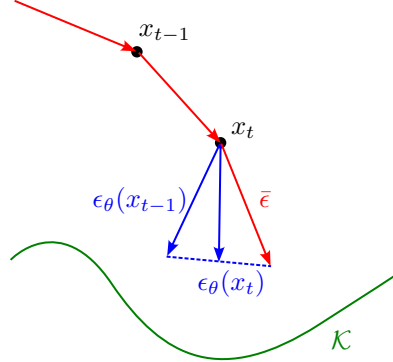


Figure 2: Illustration of our choice of  $\bar{\epsilon}_t$

Schedule	CIFAR-10	CelebA
DDIM	16.86	18.08
DDIM Offset	14.18	15.38
EDM	20.85	16.72
Ours	<b>13.25</b>	<b>13.55</b>

Table 1: FID scores of the DDIM sampler (Algorithm 1) with different  $\sigma_t$  schedules on the CIFAR-10 model for  $N = 10$  steps.

<sup>2</sup>DDIM is usually presented using not  $\sigma_t$  but parameters  $\alpha_t$  satisfying  $\sigma_t^2 = (1 - \alpha_t)/\alpha_t$ . Linear updates of  $\sigma_t$  are less natural when expressed in terms of  $\alpha_t$ .

Sampler	CIFAR-10 FID				CelebA FID			
	$N = 5$	$N = 10$	$N = 20$	$N = 50$	$N = 5$	$N = 10$	$N = 20$	$N = 50$
Ours	<b>12.53</b>	<b>3.85</b>	<b>3.39</b>	<b>3.43</b>	<b>10.73</b>	<b>4.30</b>	3.56	3.78
DDIM [43]	47.20	16.86	8.28	4.81	32.21	18.08	11.81	7.39
PNDM [24]	13.9	7.03	5.00	3.95	11.3	7.71	5.51	3.34
DPM [27]		6.37	3.72	<b>3.48</b>		5.83	<b>2.82</b>	<b>2.71</b>
DEIS [51]	18.43	7.12	4.53	3.78	25.07	6.95	3.41	2.95
UniPC [52]	23.22	<b>3.87</b>						
A-DDIM [3]		14.00	5.81*	4.04		15.62	9.22*	6.13

Table 2: FID scores of our sampler compared to that of other samplers for pretrained CIFAR-10 and CelebA models with a discrete linear schedule. The first half of the table shows our computational results whereas the second half of the table show results taken from the respective papers. \*Results for  $N = 25$

We quantitatively evaluate our sampler (Algorithm 2) by computing the Fréchet inception distance (FID) [13] between all the training images and 50k generated images. We use denoisers from [14, 43] that were pretrained on the CIFAR-10 (32x32) and CelebA (64x64) datasets [21, 26]. We compare our results with other samplers using the same denoisers. The FID scores are tabulated in Table 2, showing that our sampler achieves better performance on both CIFAR-10 (for  $N = 5, 10, 20, 50$ ) and CelebA (for  $N = 5, 10$ ).

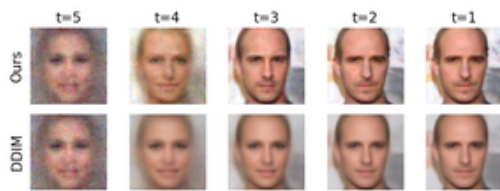


Figure 4: A comparison of our sampler with DDIM on the CelebA dataset with  $N = 5$  steps.

We also incorporated our sampler into Stable Diffusion [37] (a latent diffusion model). We change the noise schedule  $\sigma_t$  as described in Appendix E. In Figure 1, we show some results for text to image generation in  $N = 10$  function evaluations. From these experiments we can see that our sampler performs comparably to other commonly used samplers such as PNDM, UniPC and DPM++, but with the advantage of being much simpler to describe and implement.

## 6 Related Work and Discussion

**Learning diffusion models** Diffusion models were originally introduced in [42] as using a variational inference method to learn the reverse of a process that progressively adds noise to data. This approach resulted in an improved training process [14, 30] that becomes (1), which is different from the original variational lower bound. This improvement is justified from the perspective of denoising score matching [45, 46], where the  $\epsilon_\theta$  is interpreted as  $\nabla \log(p(x_t, \sigma_t))$ , the gradient of the log density of the data distribution perturbed by noise.

Score matching is also shown to be equivalent to denoising autoencoders with Gaussian noise [49]. From this derivation we can obtain a connection to our interpretation when  $\mathcal{K}$  is a finite set of training examples. The *ideal denoiser* [18] for this setting is defined as the minimizer of  $\mathbf{E}_{y \in \mathcal{K}} \mathbf{E}_{w \sim \mathcal{N}(0,1)} \|D(y + w, \sigma) - y\|^2$ , which is equivalent to a smoothed version of the projection operator (6) of  $\mathcal{K}$ , with its argmin operation replaced by a “soft argmin” induced by the log-sum-exp function.

**Sampling from diffusion models** Samplers for diffusion models started with probabilistic methods [42, 14, 30] that formed the reverse process by conditioning on the denoiser output at each step. In parallel, score based models [45, 46] interpret the forward noising process as a stochastic differential equation (SDE), so SDE solvers based on Langevin dynamics [50] are employed to reverse this process. As models get larger, computational constraints motivated the development of more efficient samplers. It is then discovered that for smaller number of sampling steps, deterministic samplers

perform better than stochastic ones [43]. These deterministic samplers are constructed by reversing a non-Markovian process that leads to the same training objective, which is also equivalent to turning the SDE into an ordinary differential equation (ODE) that matches its marginals at each sampling step [46].

This led to a large body of work focused on developing ODE and SDE solvers for fast sampling of diffusion models, a few of which we have evaluated in Table 2. Most notably, [18] put existing samplers into a common framework and isolated components that can be independently improved. Our sampler Algorithm 2 bears most similarity to linear multistep methods, which can also be interpreted as accelerated gradient descent [39]. What differs is the error model: ODE solvers aim to minimize discretization error whereas we aim to minimize gradient estimation error, resulting in different “optimal” samplers.

**Linear-inverse problems and conditioning** Several authors [17, 7, 19] have devised samplers for finding images that satisfy linear equations  $Ax = b$ . Such linear inverse problems generalize inpainting, colorization, and compressed sensing. In our framework, we can interpret this samplers as algorithms for equality constraint minimization of the distance function, a classical problem in optimization. Similarly, the widely used technique of *conditioning* [10] can be interpreted as multi-objective optimization, where minimization of distance is replaced with minimization of  $\text{dist}_{\mathcal{K}}(x)^2 + g(x)$  for an auxiliary objective function  $g(x)$ .

**Score distillation sampling** We illustrate the potential of our framework for discovering new applications of diffusion models by deriving Score Distillation Sampling (SDS), a method for parameterized optimization introduced in [32] in the context of text to 3D object generation. At a high-level, this technique finds  $(x, \theta)$  satisfying non-linear equations  $x = g(\theta)$  subject to the constraint  $x \in \mathcal{K}$ , where  $\mathcal{K}$  denotes the image manifold. It does this by iteratively updating  $x$  with a direction proportional to  $(\epsilon_{\theta}(x + \sigma\epsilon, \sigma) - \epsilon)\nabla g(\theta)$ , where  $\sigma$  is a randomly chosen noise level and  $\epsilon \sim \mathcal{N}(0, I)$ . Under our framework, this iteration can be interpreted as gradient descent on the squared distance function with gradient  $\frac{1}{2}\nabla_{\theta}\text{dist}_{\mathcal{K}}(g(\theta))^2 = (x - \text{proj}_{\mathcal{K}}(x))\nabla g(\theta)$ , with the assumption that  $\text{proj}_{\mathcal{K}}(x) \approx \text{proj}_{\mathcal{K}}(x + \sigma\epsilon)$ , along with our Section 2 denoising approximation  $\text{proj}_{\mathcal{K}}(x + \sigma\epsilon) \approx x + \sigma\epsilon - \sigma\epsilon_{\theta}(x + \sigma\epsilon, \sigma)$ .

**Learning the distance function** Reinterpreting denoising as projection, or equivalently gradient descent on the distance function, has a few immediate implications. First, it suggests generalizations that draw upon the literature for computing distance functions and projection operators. Such techniques include Fast Marching Methods [40], kd-trees, and neural-network approaches, e.g., [31, 36]. Using concentration inequalities, we can also interpret training a denoiser as learning a solution to the *Eikonal PDE*, given by  $\|\nabla d(x)\| = 1$ . Other techniques for solving this PDE with deep neural nets include [41, 23, 5].

## 7 Conclusion, Limitations and Future Work

We have presented an elementary framework for analyzing and generalizing diffusion models that has led to a new sampling approach and new interpretations of pre-existing techniques. Moreover, the key objects in our analysis—the distance function and the projection operator—are canonical objects in constrained optimization. We therefore believe our work can lead to new generative models that incorporate sophisticated objectives and constraints for a variety of applications. We also believe this work can be leveraged to incorporate existing denoisers into optimization algorithms in a plug-in-play fashion, much like the work [6, 22, 36].

The practical limitations and potential negative societal impacts of our work are inherited from that of diffusion models and image generation tools in general. The limitations of our theory include its reliance on *reach*. While estimating reach is studied [12, 1], it is unclear if the reach of practically important datasets (e.g., the image manifold) can be estimated in practice.

The correspondence between projection and denoising relies on the assumption that the manifold has low-dimension. If this assumption fails, the denoiser must be replaced with a different function that explicitly learns the projection operator. We think combining the multi-level noise paradigm of diffusion with distance function learning [31] is an interesting direction, as are diffusion-models that carry out projection using analytic formulae or simple optimization routines.

## References

- [1] AAMARI, E., KIM, J., CHAZAL, F., MICHEL, B., RINALDO, A., AND WASSERMAN, L. Estimating the reach of a manifold.
- [2] AJAY, A., DU, Y., GUPTA, A., TENENBAUM, J., JAAKKOLA, T., AND AGRAWAL, P. Is conditional generative modeling all you need for decision-making? *arXiv preprint arXiv:2211.15657* (2022).
- [3] BAO, F., LI, C., ZHU, J., AND ZHANG, B. Analytic-dpm: an analytic estimate of the optimal reverse variance in diffusion probabilistic models. *arXiv preprint arXiv:2201.06503* (2022).
- [4] BENGIO, Y., COURVILLE, A., AND VINCENT, P. Representation learning: A review and new perspectives. *IEEE transactions on pattern analysis and machine intelligence* 35, 8 (2013), 1798–1828.
- [5] BIN WAHEED, U., HAGHIGHAT, E., ALKHALIFAH, T., SONG, C., AND HAO, Q. Pinneik: Eikonal solution using physics-informed neural networks. *Computers & Geosciences* 155 (2021), 104833.
- [6] CHAN, S. H., WANG, X., AND ELGENDY, O. A. Plug-and-play admm for image restoration: Fixed-point convergence and applications. *IEEE Transactions on Computational Imaging* 3, 1 (2016), 84–98.
- [7] CHUNG, H., SIM, B., RYU, D., AND YE, J. C. Improving diffusion models for inverse problems using manifold constraints. *arXiv preprint arXiv:2206.00941* (2022).
- [8] DE BORTOLI, V. Convergence of denoising diffusion models under the manifold hypothesis. *arXiv preprint arXiv:2208.05314* (2022).
- [9] DELFOUR, M. C., AND ZOLÉSIO, J.-P. *Shapes and geometries: metrics, analysis, differential calculus, and optimization*. SIAM, 2011.
- [10] DHARIWAL, P., AND NICHOL, A. Diffusion models beat GANs on image synthesis. *Advances in Neural Information Processing Systems* 34 (2021), 8780–8794.
- [11] FEDERER, H. Curvature measures. *Transactions of the American Mathematical Society* 93, 3 (1959), 418–491.
- [12] FEFFERMAN, C., MITTER, S., AND NARAYANAN, H. Testing the manifold hypothesis. *Journal of the American Mathematical Society* 29, 4 (2016), 983–1049.
- [13] HEUSEL, M., RAMSAUER, H., UNTERTHINER, T., NESSLER, B., AND HOCHREITER, S. Gans trained by a two time-scale update rule converge to a local nash equilibrium. *Advances in neural information processing systems* 30 (2017).
- [14] HO, J., JAIN, A., AND ABBEEL, P. Denoising diffusion probabilistic models. *Advances in Neural Information Processing Systems* 33 (2020), 6840–6851.
- [15] JANNER, M., DU, Y., TENENBAUM, J. B., AND LEVINE, S. Planning with diffusion for flexible behavior synthesis. *arXiv preprint arXiv:2205.09991* (2022).
- [16] JUN, H., AND NICHOL, A. Shap-e: Generating conditional 3d implicit functions. *arXiv preprint arXiv:2305.02463* (2023).
- [17] KADKHODAIE, Z., AND SIMONCELLI, E. P. Solving linear inverse problems using the prior implicit in a denoiser. *arXiv preprint arXiv:2007.13640* (2020).
- [18] KARRAS, T., AITTALA, M., AILA, T., AND LAINE, S. Elucidating the design space of diffusion-based generative models. *arXiv preprint arXiv:2206.00364* (2022).
- [19] KAWAR, B., ELAD, M., ERMON, S., AND SONG, J. Denoising diffusion restoration models. *arXiv preprint arXiv:2201.11793* (2022).
- [20] KONG, Z., PING, W., HUANG, J., ZHAO, K., AND CATANZARO, B. Diffwave: A versatile diffusion model for audio synthesis. *arXiv preprint arXiv:2009.09761* (2020).
- [21] KRIZHEVSKY, A., HINTON, G., ET AL. Learning multiple layers of features from tiny images.
- [22] LE PENDU, M., AND GUILLEMOT, C. Preconditioned plug-and-play admm with locally adjustable denoiser for image restoration. *SIAM Journal on Imaging Sciences* 16, 1 (2023), 393–422.
- [23] LICHTENSTEIN, M., PAI, G., AND KIMMEL, R. Deep eikonal solvers. In *Scale Space and Variational Methods in Computer Vision: 7th International Conference, SSVN 2019, Hofgeismar, Germany, June 30–July 4, 2019, Proceedings* 7 (2019), Springer, pp. 38–50.
- [24] LIU, L., REN, Y., LIN, Z., AND ZHAO, Z. Pseudo numerical methods for diffusion models on manifolds. *arXiv preprint arXiv:2202.09778* (2022).
- [25] LIU, R., WU, R., VAN HOORICK, B., TOKMAKOV, P., ZAKHAROV, S., AND VONDRICK, C. Zero-1-to-3: Zero-shot one image to 3d object. *arXiv preprint arXiv:2303.11328* (2023).
- [26] LIU, Z., LUO, P., WANG, X., AND TANG, X. Deep learning face attributes in the wild. In *Proceedings of International Conference on Computer Vision (ICCV)* (December 2015).

- [27] LU, C., ZHOU, Y., BAO, F., CHEN, J., LI, C., AND ZHU, J. Dpm-solver: A fast ode solver for diffusion probabilistic model sampling in around 10 steps. *arXiv preprint arXiv:2206.00927* (2022).
- [28] LU, C., ZHOU, Y., BAO, F., CHEN, J., LI, C., AND ZHU, J. Dpm-solver++: Fast solver for guided sampling of diffusion probabilistic models. *arXiv preprint arXiv:2211.01095* (2022).
- [29] MENG, C., HE, Y., SONG, Y., SONG, J., WU, J., ZHU, J.-Y., AND ERMON, S. Sdedit: Guided image synthesis and editing with stochastic differential equations. In *International Conference on Learning Representations* (2021).
- [30] NICHOL, A. Q., AND DHARIWAL, P. Improved denoising diffusion probabilistic models. In *International Conference on Machine Learning* (2021), PMLR, pp. 8162–8171.
- [31] PARK, J. J., FLORENCE, P., STRAUB, J., NEWCOMBE, R., AND LOVEGROVE, S. Deepsdf: Learning continuous signed distance functions for shape representation. In *Proceedings of the IEEE/CVF conference on computer vision and pattern recognition* (2019), pp. 165–174.
- [32] POOLE, B., JAIN, A., BARRON, J. T., AND MILDENHALL, B. Dreamfusion: Text-to-3d using 2d diffusion. *arXiv preprint arXiv:2209.14988* (2022).
- [33] POPE, P., ZHU, C., ABDELKADER, A., GOLDBLUM, M., AND GOLDSTEIN, T. The intrinsic dimension of images and its impact on learning. *arXiv preprint arXiv:2104.08894* (2021).
- [34] POPOV, V., VOVK, I., GOGORYAN, V., SADEKOVA, T., AND KUDINOV, M. Grad-tts: A diffusion probabilistic model for text-to-speech. In *International Conference on Machine Learning* (2021), PMLR, pp. 8599–8608.
- [35] RAMESH, A., DHARIWAL, P., NICHOL, A., CHU, C., AND CHEN, M. Hierarchical text-conditional image generation with clip latents. *arXiv preprint arXiv:2204.06125* (2022).
- [36] RICK CHANG, J., LI, C.-L., POZOS, B., VIJAYA KUMAR, B., AND SANKARANARAYANAN, A. C. One network to solve them all—solving linear inverse problems using deep projection models. In *Proceedings of the IEEE International Conference on Computer Vision* (2017), pp. 5888–5897.
- [37] ROMBACH, R., BLATTMANN, A., LORENZ, D., ESSER, P., AND OMMER, B. High-resolution image synthesis with latent diffusion models. In *Proceedings of the IEEE/CVF Conference on Computer Vision and Pattern Recognition* (2022), pp. 10684–10695.
- [38] SAHARIA, C., CHAN, W., SAXENA, S., LI, L., WHANG, J., DENTON, E., GHASEMPOUR, S. K. S., AYAN, B. K., MAHDAVI, S. S., LOPES, R. G., ET AL. Photorealistic text-to-image diffusion models with deep language understanding. *arXiv preprint arXiv:2205.11487* (2022).
- [39] SCIEUR, D., ROULET, V., BACH, F., AND D’ASPREMONT, A. Integration methods and optimization algorithms. *Advances in Neural Information Processing Systems* 30 (2017).
- [40] SETHIAN, J. A. A fast marching level set method for monotonically advancing fronts. *Proceedings of the National Academy of Sciences* 93, 4 (1996), 1591–1595.
- [41] SMITH, J. D., AZIZZADENESHELI, K., AND ROSS, Z. E. Eikonet: Solving the eikonal equation with deep neural networks. *IEEE Transactions on Geoscience and Remote Sensing* 59, 12 (2020), 10685–10696.
- [42] SOHL-DICKSTEIN, J., WEISS, E., MAHESWARANATHAN, N., AND GANGULI, S. Deep unsupervised learning using nonequilibrium thermodynamics. In *International Conference on Machine Learning* (2015), PMLR, pp. 2256–2265.
- [43] SONG, J., MENG, C., AND ERMON, S. Denoising diffusion implicit models. *arXiv preprint arXiv:2010.02502* (2020).
- [44] SONG, Y., DHARIWAL, P., CHEN, M., AND SUTSKEVER, I. Consistency models. *arXiv preprint arXiv:2303.01469* (2023).
- [45] SONG, Y., AND ERMON, S. Generative modeling by estimating gradients of the data distribution. *Advances in neural information processing systems* 32 (2019).
- [46] SONG, Y., SOHL-DICKSTEIN, J., KINGMA, D. P., KUMAR, A., ERMON, S., AND POOLE, B. Score-based generative modeling through stochastic differential equations. *arXiv preprint arXiv:2011.13456* (2020).
- [47] TEVET, G., RAAB, S., GORDON, B., SHAFIR, Y., COHEN-OR, D., AND BERMANO, A. H. Human motion diffusion model. *arXiv preprint arXiv:2209.14916* (2022).
- [48] VERSHYNIN, R. *High-dimensional probability: An introduction with applications in data science*, vol. 47. Cambridge university press, 2018.
- [49] VINCENT, P. A connection between score matching and denoising autoencoders. *Neural computation* 23, 7 (2011), 1661–1674.
- [50] WELLING, M., AND TEH, Y. W. Bayesian learning via stochastic gradient langevin dynamics. In *Proceedings of the 28th international conference on machine learning (ICML-11)* (2011), Citeseer, pp. 681–688.

- [51] ZHANG, Q., AND CHEN, Y. Fast sampling of diffusion models with exponential integrator. *arXiv preprint arXiv:2204.13902* (2022).
- [52] ZHAO, W., BAI, L., RAO, Y., ZHOU, J., AND LU, J. Unipc: A unified predictor-corrector framework for fast sampling of diffusion models. *arXiv preprint arXiv:2302.04867* (2023).

## A Equivalent Definitions of DDIM and DDPM

The DDPM and DDIM samplers are usually described in a different coordinate system  $z_t$  defined by parameters  $\bar{\alpha}_t$  and the following relations, where the noise model is defined by a schedule  $\bar{\alpha}_t$ :

$$y \approx \sqrt{\bar{\alpha}_t}z + \sqrt{1 - \bar{\alpha}_t}\epsilon, \quad (13)$$

with the estimate  $\hat{z}_0^t := \hat{z}_0(z_t, t)$  given by

$$\hat{z}_0(y, t) := \frac{1}{\sqrt{\bar{\alpha}_t}}(y - \sqrt{1 - \bar{\alpha}_t}\epsilon'_\theta(y, t)). \quad (14)$$

We have the following conversion identities between the  $x$  and  $z$  coordinates:

$$x_0 = z_0, \quad x_t = z_t / \sqrt{\bar{\alpha}_t}, \quad \sigma_t = \sqrt{\frac{1 - \bar{\alpha}_t}{\bar{\alpha}_t}}, \quad \epsilon_\theta(y, \sigma_t) = \epsilon'_\theta(y / \sqrt{\bar{\alpha}_t}, t). \quad (15)$$

While this change-of-coordinates is used in [43, Section 4.3] and in [18]—and hence not new— we rigorously prove equivalence of the DDIM and DDPM samplers given in Section 1 with their original definitions.

**DDPM** Given initial  $z_N$ , the DDPM sampler constructs the sequence

$$z_{t-1} = \frac{\sqrt{\bar{\alpha}_{t-1}}(1 - \alpha_t)}{1 - \bar{\alpha}_t} \hat{z}_0^t + \frac{\sqrt{\bar{\alpha}_t}(1 - \bar{\alpha}_{t-1})}{1 - \bar{\alpha}_t} z_t + \sqrt{\frac{1 - \bar{\alpha}_{t-1}}{1 - \bar{\alpha}_t}}(1 - \alpha_t)w_t, \quad (16)$$

where  $\alpha_t := \bar{\alpha}_t / \bar{\alpha}_{t-1}$  and  $w_t \sim \mathcal{N}(0, I)$ . This is interpreted as sampling  $z_{t-1}$  from a Gaussian distribution conditioned on  $z_t$  and  $\hat{z}_0^t$  [14].

**Proposition A.1** (DDPM change of coordinates). *The sampling update (3) is equivalent to the update (16) under the change of coordinates (15).*

*Proof.* First we write (3) in terms of  $z_t$ ,  $\epsilon'_\theta(z_t, t)$  and  $w_t$  using (14):

$$\begin{aligned} z_{t-1} &= \frac{\sqrt{\bar{\alpha}_{t-1}}(1 - \alpha_t)}{\sqrt{\bar{\alpha}_t}(1 - \bar{\alpha}_t)} (z_t - \sqrt{1 - \bar{\alpha}_t}\epsilon'_\theta(z_t, t)) + \frac{\sqrt{\bar{\alpha}_t}(1 - \bar{\alpha}_{t-1})}{1 - \bar{\alpha}_t} z_t + \sqrt{\frac{1 - \bar{\alpha}_{t-1}}{1 - \bar{\alpha}_t}}(1 - \alpha_t)w_t \\ &= \frac{z_t}{\sqrt{\bar{\alpha}_t}} + \frac{\alpha_t - 1}{\sqrt{\bar{\alpha}_t}(1 - \bar{\alpha}_t)} \epsilon'_\theta(z_t, t) + \sqrt{\frac{1 - \bar{\alpha}_{t-1}}{1 - \bar{\alpha}_t}}(1 - \alpha_t)w_t. \end{aligned}$$

Next we divide both sides by  $\sqrt{\bar{\alpha}_{t-1}}$  and change  $z_t$  and  $z_{t-1}$  to  $x_t$  and  $x_{t-1}$ :

$$x_{t-1} = x_t + \frac{\alpha_t - 1}{\sqrt{\bar{\alpha}_t}(1 - \bar{\alpha}_t)} \epsilon_\theta(x_t, \sigma_t) + \sqrt{\frac{1 - \bar{\alpha}_{t-1}}{\bar{\alpha}_{t-1}}} \frac{1 - \alpha_t}{1 - \bar{\alpha}_t} w_t.$$

Now if we define

$$\begin{aligned} \eta &:= \sqrt{\frac{1 - \bar{\alpha}_{t-1}}{\bar{\alpha}_{t-1}} \frac{1 - \alpha_t}{1 - \bar{\alpha}_t}} = \sigma_{t-1} \sqrt{\frac{1 - \bar{\alpha}_t / \bar{\alpha}_{t-1}}{1 - \bar{\alpha}_t}}, \\ \sigma_{t'} &:= \sqrt{\sigma_{t-1}^2 - \eta^2} = \sigma_{t-1} \sqrt{\frac{\bar{\alpha}_t(1 / \bar{\alpha}_{t-1} - 1)}{1 - \bar{\alpha}_t}} = \frac{\sigma_{t-1}^2}{\sigma_t}, \end{aligned}$$

it remains to check that

$$\sigma_{t'} - \sigma_t = \frac{\sigma_{t-1}^2 - \sigma_t^2}{\sigma_t} = \frac{1 / \bar{\alpha}_{t-1} - 1 / \bar{\alpha}_t}{\sqrt{1 - \bar{\alpha}_t} / \sqrt{\bar{\alpha}_t}} = \frac{\alpha_t - 1}{\sqrt{\bar{\alpha}_t}(1 - \bar{\alpha}_t)}.$$

□

**DDIM** Given initial  $z_N$ , the DDIM sampler constructs the sequence

$$z_{t-1} = \sqrt{\bar{\alpha}_{t-1}} \hat{z}_0^t + \sqrt{1 - \bar{\alpha}_{t-1}} \epsilon'_\theta(z_t, t), \quad (17)$$

i.e., it estimates  $\hat{z}_0^t$  from  $z_t$  and then constructs  $z_{t-1}$  by simply updating  $\bar{\alpha}_t$  to  $\bar{\alpha}_{t-1}$ . This sequence can be equivalently expressed in terms of  $\hat{z}_0^t$  as

$$z_{t-1} = \sqrt{\bar{\alpha}_{t-1}} \hat{z}_0^t + \sqrt{\frac{1 - \bar{\alpha}_{t-1}}{1 - \bar{\alpha}_t}} (z_t - \sqrt{\bar{\alpha}_t} \hat{z}_0^t). \quad (18)$$

**Proposition A.2** (DDIM change of coordinates). *The sampling update (4) is equivalent to the update (18) under the change of coordinates (15).*

*Proof.* First we write (17) in terms of  $z_t$  and  $\epsilon'_\theta(z_t, t)$  using (14):

$$z_{t-1} = \sqrt{\frac{\bar{\alpha}_{t-1}}{\bar{\alpha}_t}} z_t + \left( \sqrt{1 - \bar{\alpha}_{t-1}} - \sqrt{\frac{\bar{\alpha}_{t-1}}{\bar{\alpha}_t}} \sqrt{1 - \bar{\alpha}_t} \right) \epsilon'_\theta(z_t, t).$$

Next we divide both sides by  $\sqrt{\bar{\alpha}_{t-1}}$  and change  $z_t$  and  $z_{t-1}$  to  $x_t$  and  $x_{t-1}$ :

$$\begin{aligned} x_{t-1} &= x_t + \left( \sqrt{\frac{1 - \bar{\alpha}_{t-1}}{\bar{\alpha}_{t-1}}} - \sqrt{\frac{\bar{\alpha}_{t-1}}{1 - \bar{\alpha}_t}} \right) \epsilon_\theta(x_t, \sigma_t) \\ &= x_t + (\sigma_{t-1} - \sigma_t) \epsilon_\theta(x_t, \sigma_t). \end{aligned}$$

□

## B Formal Comparison of Denoising and Projection

Our proof uses local Lipschitz continuity of the projection operator, stated formally as follows.

**Proposition B.1** (Theorem 6.2(vi), Chapter 6 of [9]). *Suppose  $0 < \text{reach}(\mathcal{K}) < \infty$ . Consider  $h > 0$  and  $x, y \in \mathbb{R}^n$  satisfying  $0 < h < \text{reach}(\mathcal{K})$  and  $\text{dist}_{\mathcal{K}}(x) \leq h$  and  $\text{dist}_{\mathcal{K}}(y) \leq h$ . Then the projection map satisfies  $\|\text{proj}_{\mathcal{K}}(y) - \text{proj}_{\mathcal{K}}(x)\| \leq \frac{\text{reach}(\mathcal{K})}{\text{reach}(\mathcal{K}) - h} \|y - x\|$ .*

Decomposing random noise  $w := \sigma\epsilon$  as

$$w = w_N + w_T \quad (19)$$

for  $w_N \in N_{\mathcal{K}}(x)$  and  $w_T \in N_{\mathcal{K}}(x)^\perp$  and using Lemma 2.1 allows us to show that  $\text{proj}_{\mathcal{K}}(x + w) \approx x$ .

**Theorem B.1** (Denoising vs Projection). *Fix  $\sigma > 0$  and suppose  $\mathcal{K}$  and  $t > 0$  satisfies  $\text{reach}(\mathcal{K}) > \sigma(\sqrt{n} + t)$ . Given  $x \in \mathcal{K}$  and  $\epsilon \sim \mathcal{N}(0, I)$ , let  $y = x + \sigma\epsilon$  and  $\sigma\epsilon = w_N + w_T$  by the decomposition (19). The following statements hold with probability at least  $1 - \exp(-\alpha t^2)$ , where  $\alpha > 0$  is an absolute constant.*

- (Backward error)  $x = \text{proj}_{\mathcal{K}}(y - w_T)$ .
- (Forward error)  $\|\text{proj}_{\mathcal{K}}(y) - x\| \leq C\sigma(\sqrt{d} + t)$ , where  $C = \frac{\text{reach}(\mathcal{K})}{\text{reach}(\mathcal{K}) - \sigma(\sqrt{n} + t)}$ .

*Proof.* Let  $B \in \mathbb{R}^{n \times d}$  denote an orthonormal basis for  $N_{\mathcal{K}}(x)^\perp$ , such that  $w_T = BB^T w$ ,  $\|w_T\| = \|B^T w\|$  and we have

$$\mathbf{E}[\|w_T\|^2] = \mathbf{E}[\|B^T w\|^2] + \text{Tr cov}(B^T w) = \text{Tr cov}(B^T w) = \sigma^2 \text{Tr } B^T B = \sigma^2 d. \quad (20)$$

Using a standard concentration inequality [48, page 44, Equation 3.3], we get that for a universal constant  $\alpha$ , with probability at least  $1 - \exp(-\alpha t^2)$ , we have  $\|\epsilon\| \leq \sqrt{n} + t$  and  $\|w_T\| \leq \sigma(\sqrt{d} + t)$ . Using Lemma 2.1 and the fact that  $\|w_N\| \leq \|\sigma\epsilon\| \leq \sigma(\sqrt{n} + t) < \text{reach}(\mathcal{K})$ , we get

$$\text{proj}(y - w_T) = \text{proj}(x + w_N) = x,$$

proving the first statement. To prove the second statement, we observe that

$$\begin{aligned}
\|\text{proj}(y) - x\| &= \|\text{proj}(x + w_N + w_T) - x\| \\
&= \|\text{proj}(x + w_N) - x + \text{proj}(x + w_N + w_T) - \text{proj}(x + w_N)\| \\
&= \|\text{proj}(x + w_N) - \text{proj}(x + w_N + w_T)\| \\
&\leq C\|w_T\| \\
&\leq C\sigma(\sqrt{n} + t)
\end{aligned}$$

where the second-to-last inequality comes from Proposition B.1, the assumption that  $\text{reach}(\mathcal{K}) > \sigma(\sqrt{n} + t)$ , and the inequalities  $\text{dist}_{\mathcal{K}}(x + w_N) \leq \|w_N\| \leq \sigma(\sqrt{n} + t)$  and  $\text{dist}_{\mathcal{K}}(x + w_N + w_T) \leq \|w\| \leq \sigma(\sqrt{n} + t)$ .  $\square$

## C DDIM with Projection Error Analysis

### C.1 Proof of Theorem 3.1

Make the inductive hypothesis that  $\text{dist}(x_t) = \sqrt{n}\sigma_t$ . From the definition of DDIM (4), we have

$$x_{t-1} = x_t + \left(\frac{\sigma_{t-1}}{\sigma_t} - 1\right)\sigma_t\epsilon_\theta(x_t, \sigma_t).$$

Under Assumption 1 and the inductive hypothesis, we conclude

$$\begin{aligned}
x_{t-1} &= x_t + \left(\frac{\sigma_{t-1}}{\sigma_t} - 1\right)\nabla f(x_t) \\
&= x_t - \beta_t\nabla f(x_t)
\end{aligned}$$

Using Lemma 3.1 we have that

$$\text{dist}(x_{t-1}) = (1 - \beta_t)\text{dist}(x_t) = \frac{\sigma_{t-1}}{\sigma_t}\text{dist}(x_t) = \sqrt{n}\sigma_{t-1}$$

The base case holds by assumption, proving the claim.

### C.2 Proof of Lemma 3.1

Letting  $x_0 = \text{proj}_{\mathcal{K}}(x)$  and noting  $\nabla f(x) = x - x_0$ , we have

$$\begin{aligned}
\text{dist}_{\mathcal{K}}(x_+) &= \text{dist}_{\mathcal{K}}(x + \beta(x_0 - x)) \\
&= \|x + \beta(x_0 - x) - x_0\| \\
&= \|(x - x_0)(1 - \beta)\| \\
&= (1 - \beta)\text{dist}_{\mathcal{K}}(x)
\end{aligned}$$

### C.3 Proof of Lemma 3.2

By [9, Chapter 6, Theorem 2.1],  $|\text{dist}_{\mathcal{K}}(u) - \text{dist}_{\mathcal{K}}(v)| \leq \|u - v\|$ , which is equivalent to

$$\text{dist}_{\mathcal{K}}(u) - \text{dist}_{\mathcal{K}}(v) \leq \|u - v\|, \text{dist}_{\mathcal{K}}(v) - \text{dist}_{\mathcal{K}}(u) \leq \|u - v\|.$$

Rearranging proves the claim.

### C.4 Proof of Lemma 3.3

For Item (a) we apply Lemma 3.2 at points  $u = x_+$  and  $v = x - \beta\nabla f(x)$ . We also use  $\text{dist}(v) = (1 - \beta)\text{dist}_{\mathcal{K}}(x)$ , since  $0 \leq \beta \leq 1$ , to conclude that

$$(1 - \beta)\text{dist}_{\mathcal{K}}(x) - \beta\|e\| \leq \text{dist}_{\mathcal{K}}(x_+) \leq (1 - \beta)\text{dist}_{\mathcal{K}}(x) + \beta\|e\|.$$

Using the assumption that  $\|e\| \leq \eta\text{dist}_{\mathcal{K}}(x)$  gives

$$(1 - \beta - \eta\beta)\text{dist}_{\mathcal{K}}(x) \leq \text{dist}_{\mathcal{K}}(x_+) \leq (1 - \beta + \eta\beta)\text{dist}_{\mathcal{K}}(x)$$

Simplifying completes the proof. Item (b) follows from Item (a) and induction.

### C.5 Proof of Theorem 3.2

We first state and prove an auxillary theorem:

**Theorem C.1.** Suppose Assumption 2 holds for  $\nu \geq 1$  and  $\eta > 0$ . Given  $x_N$  and  $\{\beta_t, \sigma_t\}_{t=1}^N$ , recursively define  $x_{t-1} = x_t + \beta_t \sigma_t \epsilon_\theta(x_t, t)$  and suppose that  $\text{proj}_{\mathcal{K}}(x_t)$  is a singleton for all  $t$ . Finally, suppose that  $\{\beta_t, \sigma_t\}_{t=1}^N$  satisfies  $\frac{1}{\nu} \text{dist}_{\mathcal{K}}(x_N) \leq \sqrt{n} \sigma_N \leq \nu \text{dist}_{\mathcal{K}}(x_N)$  and

$$\frac{1}{\nu} \text{dist}_{\mathcal{K}}(x_N) \prod_{i=t}^N (1 + \beta_i(\eta - 1)) \leq \sqrt{n} \sigma_{t-1} \leq \nu \text{dist}_{\mathcal{K}}(x_N) \prod_{i=t}^N (1 - \beta_i(\eta + 1)). \quad (21)$$

The following statements hold.

- $\text{dist}_{\mathcal{K}}(x_N) \prod_{i=t}^N (1 - \beta_i(\eta + 1)) \leq \text{dist}_{\mathcal{K}}(x_{t-1}) \leq \text{dist}_{\mathcal{K}}(x_N) \prod_{i=t}^N (1 + \beta_i(\eta - 1))$
- $\frac{1}{\nu} \text{dist}_{\mathcal{K}}(x_{t-1}) \leq \sqrt{n} \sigma_{t-1} \leq \nu \text{dist}_{\mathcal{K}}(x_{t-1})$

*Proof.* Since  $\text{proj}_{\mathcal{K}}(x_t)$  is a singleton,  $\nabla f(x_t)$  exists. Hence, the result will follow from Lemma 3.3-(b) if we can show that  $\|\beta_t \sigma_t \epsilon_\theta(x_t, t) - \nabla f(x_t)\| \leq \eta \text{dist}_{\mathcal{K}}(x_t)$ . Under Assumption 2, it suffices to show that

$$\frac{1}{\nu} \text{dist}_{\mathcal{K}}(x_t) \leq \sqrt{n} \sigma_t \leq \nu \text{dist}_{\mathcal{K}}(x_t) \quad (22)$$

holds for all  $t$ . We use induction, noting that the base case ( $t = N$ ) holds by assumption. Suppose then that (22) holds for all  $t, t+1, \dots, N$ . By Lemma 3.3 and Assumption 2, we have

$$\text{dist}_{\mathcal{K}}(x_N) \prod_{i=t}^N (1 - \beta_i(\eta + 1)) \leq \text{dist}_{\mathcal{K}}(x_{t-1}) \leq \text{dist}_{\mathcal{K}}(x_N) \prod_{i=t}^N (1 + (\eta - 1)\beta_i)$$

Combined with (21) shows

$$\frac{1}{\nu} \text{dist}_{\mathcal{K}}(x_{t-1}) \leq \sqrt{n} \sigma_{t-1} \leq \nu \text{dist}_{\mathcal{K}}(x_{t-1}),$$

proving the claim.  $\square$

The proof of Theorem 3.2 follows that of Theorem C.1 by additionally observing  $\eta < 1$  implies that  $\text{dist}_{\mathcal{K}}(x_t) < \text{reach}(\mathcal{K})$  for all  $t$ , which implies  $\text{proj}_{\mathcal{K}}(x_t)$  is a singleton.

### C.6 Proof of Theorem 3.3

Assuming constant step-size  $\beta_i = \beta$  and dividing (7) by  $\prod_{i=1}^N (1 - \beta)$  gives the conditions

$$\left(1 + \eta \frac{\beta}{1 - \beta}\right)^N \leq \nu, \quad \left(1 - \eta \frac{\beta}{1 - \beta}\right)^N \geq \frac{1}{\nu}.$$

Rearranging and defining  $a = \eta \frac{\beta}{1 - \beta}$  and  $b = \nu^{\frac{1}{N}}$  gives

$$a \leq b - 1, \quad a \leq 1 - b^{-1}.$$

Since  $b - 1 - (1 - b^{-1}) = b + b^{-1} - 2 \geq 0$  for all  $b > 0$ , we conclude  $a \leq b - 1$  holds if  $a \leq 1 - b^{-1}$  holds. We therefore consider the second inequality  $\eta \frac{\beta}{1 - \beta} \leq 1 - \nu^{-1/N}$ , noting that it holds for all  $0 \leq \beta < 1$  if and only if  $0 \leq \beta \leq \frac{k}{1+k}$  for  $k = \frac{1}{\eta}(1 - \nu^{-1/N})$ , proving the claim.

### C.7 Proof of Theorem 3.4

The value of  $\sigma_0/\sigma_N$  follows from the definition of  $\sigma_t$  and the upper bound for  $\text{dist}_{\mathcal{K}}(x_0)/\text{dist}_{\mathcal{K}}(x_N)$  follows from Theorem 3.3. We introduce the parameter  $\mu$  to get a general form of the expression inside the limit:

$$(1 - \mu \beta_{*,N})^N = \left(1 - \mu \frac{1 - \nu^{-1/N}}{\eta + 1 - \nu^{-1/N}}\right)^N.$$

Next we take the limit using L'Hôpital's rule:

$$\begin{aligned}
\lim_{N \rightarrow \infty} \left( 1 - \mu \frac{1 - \nu^{-1/N}}{\eta + 1 - \nu^{-1/N}} \right)^N &= \exp \left( \lim_{N \rightarrow \infty} \log \left( 1 - \mu \frac{1 - \nu^{-1/N}}{\eta + 1 - \nu^{-1/N}} \right) / (1/N) \right) \\
&= \exp \left( \lim_{N \rightarrow \infty} \frac{\eta \mu \log(\nu)}{(\nu^{-1/N} - \eta - 1)(\nu^{1/N}(\eta - \mu + 1) + \mu - 1)} \right) \\
&= \exp \left( -\frac{\mu \log(\nu)}{\eta} \right) \\
&= (1/\nu)^{\mu/\eta}.
\end{aligned}$$

For the first limit, we set  $\mu = 1$  to get

$$\lim_{N \rightarrow \infty} (1 - \beta_{*,N})^N = (1/\nu)^{1/\eta}.$$

For the second limit, we set  $\mu = 1 - \eta$  to get

$$\lim_{N \rightarrow \infty} (1 + (\eta - 1)\beta_{*,N})^N = (1/\nu)^{\frac{1-\eta}{\eta}}.$$

## C.8 Denoiser Error

Assumption 2 places a condition directly on the approximation of  $\nabla f(x)$ , where  $f(x) := \frac{1}{2} \text{dist}_{\mathcal{K}}(x)$ , that is jointly obtained from  $\bar{\alpha}_t$  and the denoiser  $\epsilon_\theta$ . We prove this assumption holds under a direct assumption on  $\nabla \text{dist}_{\mathcal{K}}(x)$ , which is easier to verify in practice.

**Assumption 3.** *There exists  $\nu \geq 1$  and  $\eta > 0$  such that if  $\frac{1}{\nu} \text{dist}_{\mathcal{K}}(x) \leq \sqrt{n} \sigma_t \leq \nu \text{dist}_{\mathcal{K}}(x)$  then  $\|\epsilon_\theta(x, t) - \sqrt{n} \nabla \text{dist}_{\mathcal{K}}(x)\| \leq \eta$*

**Lemma C.1.** *If Assumption 3 holds with  $(\nu, \eta)$ , then Assumption 2 holds with  $(\hat{\nu}, \hat{\eta})$ , where  $\hat{\eta} = \frac{1}{\sqrt{n}} \eta \nu + \max(\nu - 1, 1 - \frac{1}{\nu})$  and  $\hat{\nu} = \nu$ .*

*Proof.* Multiplying the error-bound on  $\epsilon_\theta$  by  $\sigma_t$  and using  $\sqrt{n} \sigma_t \leq \nu \text{dist}_{\mathcal{K}}(x)$  gives

$$\|\sigma_t \epsilon_\theta(x, t) - \sqrt{n} \sigma_t \nabla \text{dist}_{\mathcal{K}}(x)\| \leq \eta \sigma_t \leq \eta \nu \frac{1}{\sqrt{n}} \text{dist}_{\mathcal{K}}(x)$$

Defining  $C = \sqrt{n} \sigma_t - \text{dist}_{\mathcal{K}}(x)$  and simplifying gives

$$\begin{aligned}
\eta \nu \frac{1}{\sqrt{n}} \text{dist}_{\mathcal{K}}(x) &\geq \|\sigma_t \epsilon_\theta(x, t) - \sqrt{n} \sigma_t \nabla \text{dist}_{\mathcal{K}}(x)\| \\
&= \|\sigma_t \epsilon_\theta(x, t) - \nabla f(x) - C \nabla \text{dist}_{\mathcal{K}}(x)\| \\
&\geq \|\sigma_t \epsilon_\theta(x, t) - \nabla f(x)\| - \|C \nabla \text{dist}_{\mathcal{K}}(x)\| \\
&= \|\sigma_t \epsilon_\theta(x, t) - \nabla f(x)\| - |C|
\end{aligned}$$

Since  $(\frac{1}{\nu} - 1) \text{dist}_{\mathcal{K}}(x) \leq C \leq (\nu - 1) \text{dist}_{\mathcal{K}}(x)$  and  $\nu \geq 1$ , the Assumption 2 error bound holds for the claimed  $\hat{\eta}$ .  $\square$

## D Further Experiments

### D.1 Distance Function Properties

We test Assumption 1 and Assumption 2 on pretrained networks. If Assumption 1 is true, then  $\|\epsilon_\theta(x_t, \sigma_t)\| \sqrt{n} = \|\nabla \text{dist}_{\mathcal{K}}(x_t)\| = 1$  for every  $x_t$  along the DDIM trajectory. In Figure 5a, we plot the distribution of norm of the denoiser  $\epsilon_\theta(x_t, \sigma_t)$  over the course of many runs of the DDIM sampler on the CIFAR-10 model for  $N = 100$  steps ( $t = 1000, 990, \dots, 20, 10, 0$ ). This plot shows that  $\|\epsilon_\theta(x_t, \sigma_t)\| / \sqrt{n}$  stays approximately constant and is close to 1 until the end of the sampling process. We next test Assumption 3, which implies Assumption 2 by Lemma C.1. We do this by first sampling a fixed noise vector  $\epsilon$ , next adding different levels of noise  $\sigma_t$ , then using the denoiser to predict  $\epsilon_\theta(x_0 + \sigma_t \epsilon, \sigma_t)$ . In Figure 5b, we plot the distribution of  $\|\epsilon_\theta(x_0 + \sigma_t \epsilon, \sigma_t) - \epsilon\| / \sqrt{n}$  over different levels of  $t$ , as a measure of how well the denoiser predicts the added noise.

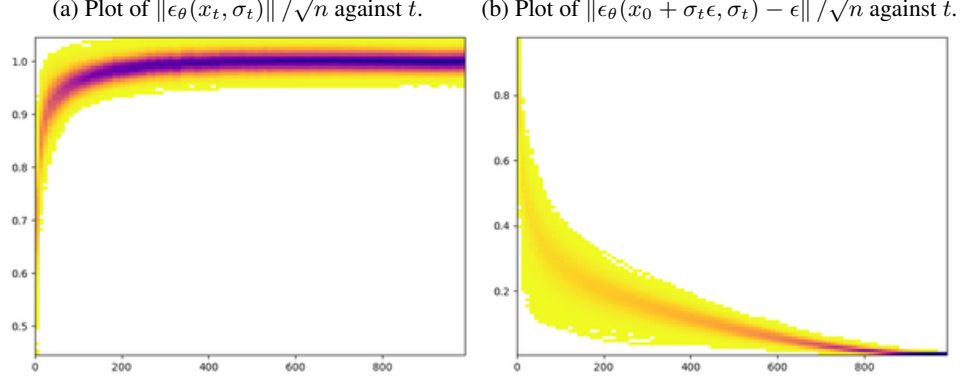


Figure 5: Plots of the norm of the denoiser at different stages of denoising, as well as the ability of the denoiser to accurately predict the added noise as a function of noise added.

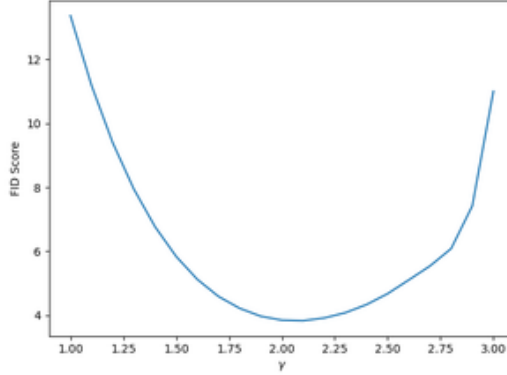


Figure 6: Plot of FID score against  $\gamma$  for our second-order sampling algorithm on the CIFAR-10 dataset for  $N = 10$  steps.

## D.2 Choice of $\gamma$

We motivate our choice of  $\gamma = 2$  in Algorithm 2 with the following experiment. In Figure 6 we plot FID scores of our sampler on the CIFAR-10 model for  $N = 10$  timesteps, using our  $\sigma_t$  schedule described in Appendix E.3, while varying  $\gamma$ . This justifies our choice of  $\gamma = 2$  to achieve the optimal FID score. Further experiments also show that the optimal value of  $\gamma$  stays constant over different datasets and choices of  $N$ .

## E Experiment Details

### E.1 Pretrained Models

The CIFAR-10 model and architecture were based on that in [14], and the CelebA model and architecture were based on that in [43]. The specific checkpoints we use are provided by [24]. We also use Stable Diffusion 2.1 provided in <https://huggingface.co/stabilityai/stable-diffusion-2-1>.

### E.2 FID Score Calculation

We generate 50000 images using our sampler and calculate the FID score using the library in <https://github.com/mseitzer/pytorch-fid>. The statistics on the training dataset were obtained from the files provided by [24].

### E.3 Our Selection of $\sigma_t$

Let  $\sigma_1^{\text{DDIM}(N)}$  be the noise level at  $t = 1$  for the DDIM sampler with  $N$  steps. For the CIFAR-10 and CelebA models, we choose  $\sigma_1 = \sqrt{\sigma_1^{\text{DDIM}(N)}}$  and  $\sigma_0 = 0.01$ . For CIFAR-10  $N = 5, 10, 20, 50$  and CelebA  $N = 5$  we choose  $\sigma_N = 40$  and for CelebA  $N = 10, 20, 50$  we choose  $\sigma_N = 80$ . For Stable Diffusion, we choose  $\sigma_N = 14.6$ ,  $\sigma_1 = \sigma_1^{\text{DDIM}(N)}$  and  $\sigma_0 = 0.0292$ .

### E.4 Text Prompts

For the text to image generation in Figure 1, the text prompts used are:

- “A digital Illustration of the Babel tower, 4k, detailed, trending in artstation, fantasy vivid colors”
- “London luxurious interior living-room, light walls”
- “Cluttered house in the woods, anime, oil painting, high resolution, cottagecore, ghibli inspired, 4k”